



Chrysanthemum indicum microparticles on removal of hazardous Congo red dye using response surface methodology

J. Chukki¹ · S. Abinandan² · S. Shanthakumar¹ 

Received: 19 June 2018 / Accepted: 8 November 2018 / Published online: 17 November 2018
© The Author(s) 2018

Abstract

Biomass-derived adsorbents have been intensively studied due to their competence in reducing pollutants with conventional methods. Flowers are used as source in medicine, cosmetics and even as adsorbents for pollutant abatement. In this study, the microparticles from *Chrysanthemum indicum* were used as adsorbent for reducing the Congo red dye concentration from synthetic solution. Batch trials were evaluated to understand the influence of factors and optimization was carried out using central composite design. Maximum reduction (84.1%) achieved under the optimized settings of pH (1.0), adsorbent dose (300 ppm), stirring speed (150 rpm), and contact time (75 min) at initial dye concentration (150 ppm at 30 °C). Microparticle size ensured with surface morphology of the adsorbent using electron microscopy and functional groups was studied using infrared spectroscopy techniques, respectively. Regression coefficient (R^2) value was obtained as 0.956 which indicates that the predicted values were in good agreement with their corresponding experimental values for the Congo red dye adsorption. Based on the investigation, it is inferred that the *Chrysanthemum indicum* flower has the potential for Congo red dye reduction from aqueous solution.

Keywords Congo red dye · *Chrysanthemum indicum* · Adsorption · Central composite design

Introduction

Several industries extensively use synthetic dyes and generate a large volume of dye effluent. This dye effluent contains enormous salt and organic content and they are less biodegradable. Discharge of these dyes into natural water system without the treatment results in ecological imbalance [1–4]. Synthetic dyes are resistance to the physicochemical reaction and have thermal and optical stability due to the complex aromatic structure [5, 6]. By conventional methods, it is challenging to treat the wastewater which contains dyes [7, 8]. Azo dyes account for 60–70% of total dye consumption in many industries [7]. Congo red (CR) is the synthetic anionic azo dye [9] and the effluent had to be adequately treated and discharged into the environment, otherwise it can metabolize into benzidine, which is a human carcinogen

[10]. CR dye contains complex aromatic structure which complicates the treatment process. It has thermal and optical stability, and resistance to biodegradation and photodegradation [11]. CR dye is used for staining purpose and as a pH indicator in the laboratory. It is also used for detecting bacteria, amyloidosis diagnosis and to treat protein folding disorders, dermatological disorders, neurodegenerative diseases, etc. However, CR dye causes allergic reactions and it is a cytotoxic, genotoxic, hematotoxic, neurotoxic, as well as mutagenic substance [12, 13]. Generally, chemical oxidation, ozonisation, membrane filtration, ion exchange or electrochemical techniques are the different methods used to treat dye-contaminated wastewater. Adsorption is proved to be the best method compared to all other technologies due to its less capital outlay. Detailed literature review shows that various adsorbents were used for Congo red dye removal from wastewater, which includes polypyrrole–polyaniline nanofibers [14], modified zeolites [2], sugarcane bagasse [15], aniline propyl silica xerogel [16], tamarind fruit shell [17], acrylamide–sodium dodecyl sulfate layered double hydroxides [18], mesoporous ZrO_2 fibers [19], ammonium aluminum carbonate hydroxide–nickel hydroxide composite [20], zinc oxide–alumina composite [21], nickel cobaltite

✉ S. Shanthakumar
shanthakumar.s@vit.ac.in

¹ Department of Environmental and Water Resources Engineering, School of Civil Engineering, Vellore Institute of Technology (VIT), Vellore 632014, India

² Eco Tech Labs Private Limited, Chennai 600032, India

[22] and *Funalia trogii* [23]. However, some of these are not effective for the anionic dye. The biosorbent (*Chrysanthemum indicum*) belongs to *Asteraceae* family and are known as Indian chrysanthemum which are widely used for decoration purposes [24, 25]. Further, the literature review indicates that *Chrysanthemum indicum* flowers (CIF) which are used in this study as an adsorbent for CR dye removal have not yet been studied previously. In India, CIF is generally used for the ornamental purpose and the regular return of CIF is 16.7 tons/hectare that is reported in our previous study [26]. The main aim deals with CIF ability as an adsorbent to treat synthetic CR dye wastewater. CCD is widely adapted to observe the effect of individual process factors and their interactive effects.

Materials and methods

Microparticles

CIF was obtained from the native marketplaces of Vellore district, Tamil Nadu, India and meticulously washed to remove dust and dirt particles. Petals were collected and dried and powdered using a domestic mixer. This powder was sieved. Particles of size less than 100 microns were further used as an adsorbent. Physical characteristics of the microparticles are presented elsewhere [26].

Dye

Congo red (CR) dye ($C_{32}H_{22}N_6Na_2O_6S_2$; MW- 696.665; $\lambda_{max} = 497$ nm) working derivative solutions made appropriately by diluting the stock solution (1 mg mL^{-1}) with double distilled water.

Adsorption experiment

Experimental trials were carried based on the procedure mentioned in our previous studies [26]. 250-mL Erlenmeyer flasks were used with 100 mL of CR dye solution based on the experimental run generated as mentioned in Table 1. Changes in the reduction were analyzed in the residual supernatant obtained after centrifugation (8000 rpm for 10 min) by UV–Vis spectrophotometer ($\lambda = 497$ nm). Percentage dye reduction was calculated using the following equation:

Table 1 Level of independent variables and experimental range

Independent variables	Design variables	Range and levels		
		−1	0	+1
pH	F ₁	4	6	8
Adsorbent dose(g/L)	F ₂	2	3	4
Initial dye conc. (mg/L)	F ₃	100	150	200
RPM	F ₄	100	150	200
Contact time (min)	F ₅	60	75	90
Temperature (°C)	F ₆	25	30	35

$$\text{Percentage reduction} = \left[\frac{(C_i - C_f)}{C_i} \right] \times 100,$$

where C_i , C_f are the initial and final dye concentrations (mg L^{-1}), respectively.

Experimental design

In tradition method of adsorption, variable response effect is studied by varying one variable at a time, ending up in large experimental trails associated with high time consumption process without representing the interaction effect between factors. Therefore, RSM is considered as one of the most useful methods for optimizing the process and portray the influence by several parameters [27, 28]. The experimental trails are carried out based on the quadratic equation (Eq. 1) between the independent variable and coefficients of central composite design (CCD), as expressed below:

$$y = \mu_0 + \mu_1 F_1 + \mu_2 F_2 + \dots + \mu_n F_n \pm c, \quad (1)$$

where y is the response (yield), μ is the response function, c is the error, and $F_1, F_2, F_3 \dots F_n$ are the independent process parameters.

Results and discussion

Central composite design

Based on CCD principle, the design of six variables consists of 53 experiments that are calculated by the following expression:

$$N = 2^{M-1} + 2M + f_0, \quad (2)$$

where N is an experimental trail, M is the independent variables, and f_0 is the central points.

Table 1 shows the independent variables and their experimental range. Table 2 shows the 2^6 fractional factorial design CCD matrix.

Equation 2 is expanded to Eq 3 for a six-variable design:

Table 2 Fractional factorial CCD matrix with code and real variables

Run	F ₁	F ₂	F ₃	F ₄	F ₅	F ₆	pH	Ads. dose (g/L)	Ini.dye conc. (mg/L)	RPM	Contact time (min.)	Temp. (°C)
1	0	0	0	2	0	0	6	3.0	150	270	75	30
2	1	1	-1	1	1	-1	8	4.0	100	200	90	25
3	0	-2	0	0	0	0	6	0.6	150	150	75	30
4	0	0	0	0	0	0	6	3.0	150	150	75	30
5	1	1	1	-1	1	-1	8	4.0	200	100	90	25
6	0	0	0	0	0	-2	6	3.0	150	150	75	18
7	-1	1	-1	-1	-1	1	4	4.0	100	100	60	35
8	1	-1	-1	1	1	1	8	2.0	100	200	90	35
9	0	0	0	0	0	2	6	3.0	150	150	75	42
10	0	2	0	0	0	0	6	5.4	150	150	75	30
11	-1	-1	1	1	1	1	4	2.0	200	200	90	35
12	1	-1	1	-1	1	1	8	2.0	200	100	90	35
13	0	0	0	0	0	0	6	3.0	150	150	75	30
14	0	0	2	0	0	0	6	3.0	270	150	75	30
15	-1	-1	-1	-1	-1	-1	4	2.0	100	100	60	25
16	1	1	-1	-1	-1	-1	8	4.0	100	100	60	25
17	1	1	-1	1	-1	1	8	4.0	100	200	60	35
18	0	0	0	0	0	0	6	3.0	150	150	75	30
19	1	-1	1	-1	-1	-1	8	2.0	200	100	60	25
20	1	-1	1	1	-1	1	8	2.0	200	200	60	35
21	1	-1	-1	-1	-1	1	8	2.0	100	100	60	35
22	-1	1	-1	1	1	1	4	4.0	100	200	90	35
23	-1	-1	1	-1	-1	1	4	2.0	200	100	60	35
24	-1	1	1	-1	1	1	4	4.0	200	100	90	35
25	1	1	1	1	-1	-1	8	4.0	200	200	60	25
26	0	0	0	-2	0	0	6	3.0	150	30	75	30
27	0	0	0	0	0	0	6	3.0	150	150	75	30
28	1	1	-1	-1	1	1	8	4.0	100	100	90	35
29	-1	-1	-1	1	-1	1	4	2.0	100	200	60	35
30	-1	1	1	1	-1	1	4	4.0	200	200	60	35
31	1	1	1	1	1	1	8	4.0	200	200	90	35
32	1	-1	-1	-1	1	-1	8	2.0	100	100	90	25
33	1	-1	-1	1	-1	-1	8	2.0	100	200	60	25
34	0	0	0	0	0	0	6	3.0	150	150	75	30
35	0	0	0	0	0	0	6	3.0	150	150	75	30
36	1	-1	1	1	1	-1	8	2.0	200	200	90	25
37	0	0	0	0	-2	0	6	3.0	150	150	40	30
38	0	0	0	0	0	0	6	3.0	150	150	75	30
39	2	0	0	0	0	0	11	3.0	150	150	75	30
40	0	0	-2	0	0	0	6	3.0	30	150	75	30
41	-1	1	1	-1	-1	-1	4	4.0	200	100	60	25
42	0	0	0	0	2	0	6	3.0	150	150	110	30
43	0	0	0	0	0	0	6	3.0	150	150	75	30
44	-1	-1	-1	-1	1	1	4	2.0	100	100	90	35
45	-1	-1	1	-1	1	-1	4	2.0	200	100	90	25
46	-1	-1	1	1	-1	-1	4	2.0	200	200	60	25
47	-1	1	-1	1	-1	-1	4	4.0	100	200	60	25
48	-1	1	1	1	1	-1	4	4.0	200	200	90	25
49	-1	1	-1	-1	1	-1	4	4.0	100	100	90	25



Table 2 (continued)

Run	F ₁	F ₂	F ₃	F ₄	F ₅	F ₆	pH	Ads. dose (g/L)	Ini.dye conc. (mg/L)	RPM	Contact time (min.)	Temp. (°C)
50	-1	-1	-1	1	1	-1	4	2.0	100	200	90	25
51	1	1	1	-1	-1	1	8	4.0	200	100	60	35
52	-2	0	0	0	0	0	1	3.0	150	150	75	30
53	0	0	0	0	0	0	6	3.0	150	150	75	30

$$\begin{aligned}
 y = & \mu_0 + \mu_1 F_1 + \mu_2 F_2 + \mu_3 F_3 + \mu_4 F_4 + \mu_5 F_5 \\
 & + \mu_{11} F_{12} + \mu_{22} F_{22} + \mu_{33} F_{32} + \mu_{44} F_{42} \\
 & + \mu_{55} F_{52} + \mu_{66} F_{62} + \mu_{12} F_1 F_2 + \mu_{13} F_1 F_3 \\
 & + \mu_{14} F_1 F_4 + \mu_{15} F_1 F_5 + \mu_{16} F_1 F_6 + \mu_{23} F_2 F_3 \\
 & + \mu_{24} F_2 F_4 + \mu_{25} F_2 F_5 + \mu_{26} F_2 F_6 + \mu_{34} F_3 F_4 \\
 & + \mu_{35} F_3 F_5 + \mu_{36} F_3 F_6 + \mu_{45} F_4 F_5 + \mu_{46} F_4 F_6 \\
 & + \mu_{56} F_5 F_6,
 \end{aligned} \quad (3)$$

where y is the dye removal (%); F_1, F_2, F_3, F_4, F_5 are the independent variables; μ_0 is the regression coefficient; $\mu_1, \mu_2, \mu_3, \mu_4, \mu_5, \mu_6$ are the linear coefficients; $\mu_{11}, \mu_{22}, \mu_{33}, \mu_{44}, \mu_{55}, \mu_{66}$ are the quadratic coefficients; and $\mu_{12}, \mu_{13}, \mu_{14}, \mu_{15}, \mu_{16}, \mu_{23}, \mu_{24}, \mu_{25}, \mu_{26}, \mu_{34}, \mu_{35}, \mu_{36}, \mu_{45}, \mu_{46}, \mu_{56}$ are the interaction coefficients.

With the coefficients in Eq 3:

$$\begin{aligned}
 y = & 59.3528 - 3.8176F_1 + 5.9990F_2 - 3.1209F_3 \\
 & + 0.7326F_4 + 2.1713F_5 - 0.4646F_6 \\
 & + 2.0057F_{12} - 0.4492F_{22} + 0.7676F_{32} \\
 & - 0.6081F_{42} - 1.1907F_{52} + 1.3164F_{62} \\
 & - 0.0364F_1 F_2 + .9034F_1 F_3 - 0.2190F_1 F_4 \\
 & + 4.3763F_1 F_5 - 1.1797F_1 F_6 + 1.0092F_2 F_3 \\
 & - 0.5795F_2 F_4 + 3.4821F_2 F_5 + 0.3418F_2 F_6 \\
 & + 2.7554F_3 F_4 - 1.0721F_3 F_5 + 1.4783F_3 F_6 \\
 & + 0.4062F_4 F_5 - 2.2752F_4 F_6 + 0.5504F_5 F_6.
 \end{aligned} \quad (4)$$

Microparticle characteristics

The morphology of pre- and post-treated adsorbents surface was studied using scanning electron microscopic technique and presented in Fig. 1. It can be observed from the figure that the surface of the adsorbent was irregular and multifarious in nature. In addition, the particles are asymmetric and the uneven surface increases the physical adsorption. FTIR spectrum depicts the functional groups present in the adsorbent [29]. Figure 2 shows the FTIR spectra ranging between 400 and 4000 cm^{-1} of adsorbent pre- and post-experimental trails. In Fig. 2, the peaks at wavenumbers 1737.8 and 1600.9 cm^{-1} indicate the presence of C=O group. Broad absorption near 3400–2400 cm^{-1} confirms the occurrence of O–H group.

Strong intensity absorptions near 1300–1000 cm^{-1} show the presence of esters(C–O group). Some functional group's peaks in figure are shifted after adsorption. The downshift of the wavenumber from 1600 to 1641 cm^{-1} indicates the bending vibrations of N–H group in the adsorption process. The intensity of peaks at the regions 1737 cm^{-1} , 1641 cm^{-1} , 1429 cm^{-1} , 1365 cm^{-1} , 1228 cm^{-1} , 1149 cm^{-1} significantly shifted due to the adsorbent contact with CR, indicating the complexation and attachment to the surface of the dye

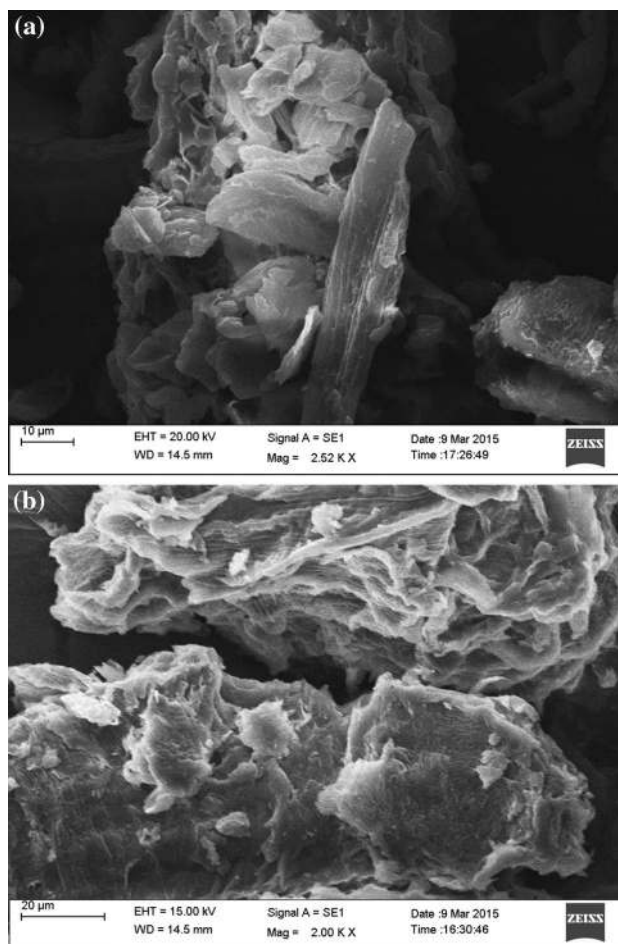


Fig. 1 SEM images of **a** raw and **b** CR dye-loaded adsorbent

Fig. 2 FTIR spectra of **a** raw and **b** CR dye-loaded adsorbent

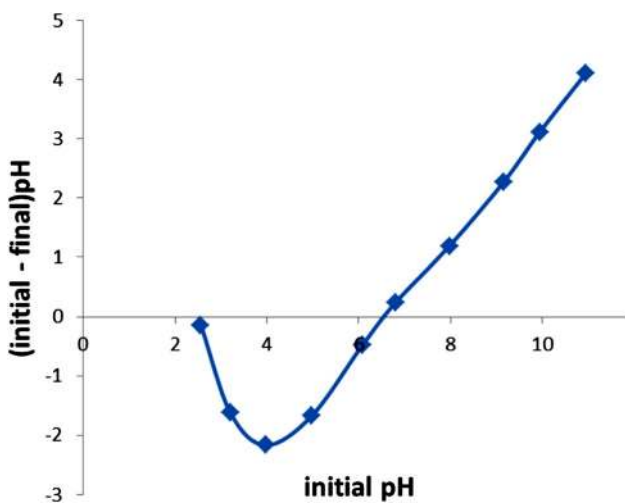
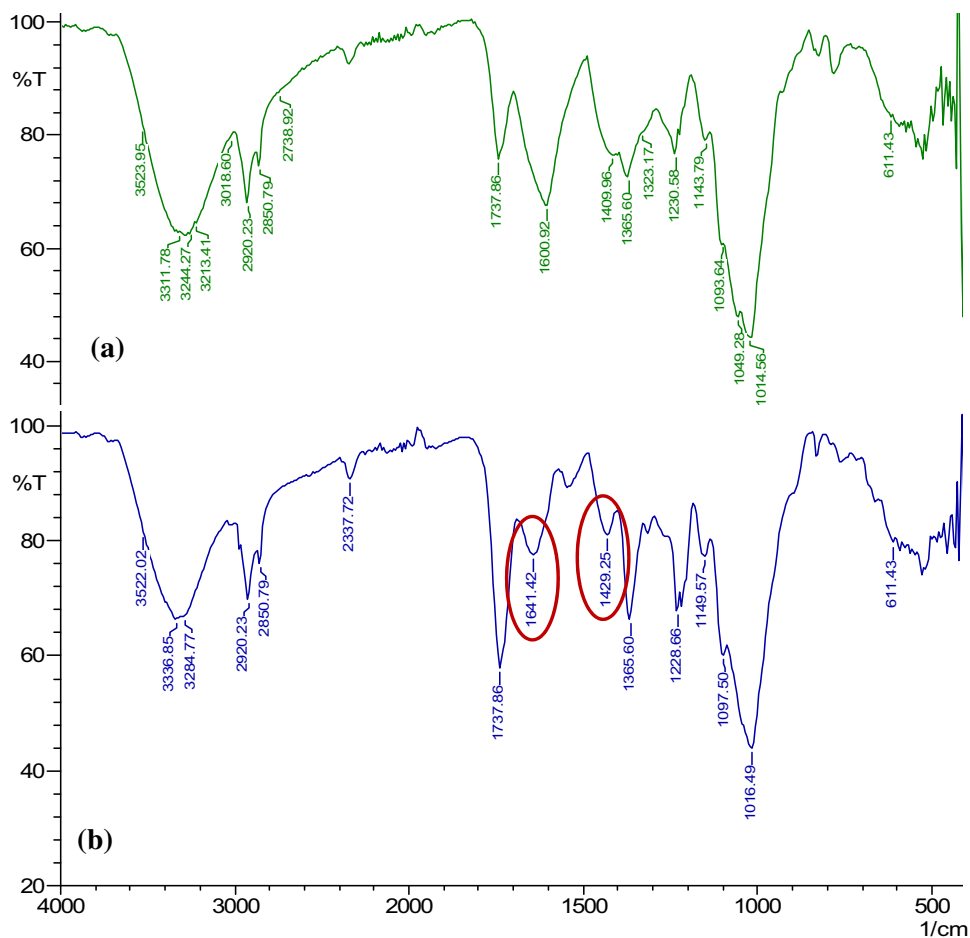


Fig. 3 Point of zero charge

Point of zero charge (PZC)

PZC is to determine the pH influence on CR dye removal. 100 mL of double distilled water has taken in conical

flasks. Adjust the pH of all flasks from 2 to 10 using 0.1 N NaOH and 0.1 N HCl and take as initial pH. Add 0.1 g of adsorbent to all flasks and agitated at 120 rpm for 24 h. Measure the pH after equilibrium which has been considered as final pH. Plot the graph of initial pH vs difference in initial and final pH values. The pH at which it is zero is considered as PZC value. From Fig. 3, it is noted that PZC value of CI is 6.6. This shows that at pH < 6.6, CI adsorbent carries positive surface charge, whereas at pH > 6.6 adsorbent carries negative surface charge.

Response surface methodology

Table 1 shows the independent variables and their experimental range. Table 2 shows the 2⁶ fractional factorial design CCD matrix, whereas Table 3 depicts the experimental results and predicted. Analysis of variance (ANOVA) which is used in evaluating adequacy and significance of the model is shown in Table 4. Values from the ANOVA table indicate that all variables and their interactions are significant. Degree of significance of each variable is represented by *p* value and variation of the data about its mean is described by *F*-value [30]. *R*² (0.9569) value shows the

Table 3 Fractional factorial CCD matrix and the output response for dye removal

Run	pH	Ads. dose (g/L)	Ini.dye conc. (mg/L)	Rpm	Contact time (min.)	Temp. (°C)	Dye removal (%) exp.	Dye removal (%) pre.
1	6	3.0	150	270	75	30	57.453	57.655
2	8	4.0	100	200	90	25	78.727	76.740
3	6	0.6	150	150	75	30	43.870	42.544
4	6	3.0	150	150	75	30	57.453	59.353
5	8	4.0	200	100	90	25	66.742	65.992
6	6	3.0	150	150	75	18	71.336	67.904
7	4	4.0	100	100	60	35	75.581	76.806
8	8	2.0	100	200	90	35	52.360	51.333
9	6	3.0	150	150	75	42	64.644	65.694
10	6	5.4	150	150	75	30	72.135	71.080
11	4	2.0	200	200	90	35	52.734	51.004
12	8	2.0	200	100	90	35	48.689	49.244
13	6	3.0	150	150	75	30	59.750	59.353
14	6	3.0	270	150	75	30	53.814	56.272
15	4	2.0	100	100	60	25	69.432	70.636
16	8	4.0	100	100	60	25	54.157	56.730
17	8	4.0	100	200	60	35	39.255	43.612
18	6	3.0	150	150	75	30	56.954	59.353
19	8	2.0	200	100	60	25	41.798	42.535
20	8	2.0	200	200	60	35	49.213	47.303
21	8	2.0	100	100	60	35	50.262	49.832
22	4	4.0	100	200	90	35	73.184	73.288
23	4	2.0	200	100	60	35	56.570	59.399
24	4	4.0	200	100	90	35	67.640	69.065
25	8	4.0	200	200	60	25	59.251	59.107
26	6	3.0	150	30	75	30	56.754	54.171
27	6	3.0	150	150	75	30	59.151	59.353
28	8	4.0	100	100	90	35	78.876	77.109
29	4	2.0	100	200	60	35	62.472	64.064
30	4	4.0	200	200	60	35	71.236	69.258
31	8	4.0	200	200	90	35	73.997	73.635
32	8	2.0	100	100	90	25	56.854	59.674
33	8	2.0	100	200	60	25	54.307	53.725
34	6	3.0	150	150	75	30	58.452	59.353
35	6	3.0	150	150	75	30	60.949	59.353
36	8	2.0	200	200	90	25	58.052	57.668
37	6	3.0	150	150	40	30	50.762	47.453
38	6	3.0	150	150	75	30	62.347	59.353
39	11	3.0	150	150	75	30	59.656	61.619
40	6	3.0	30	150	75	30	75.958	71.118
41	4	4.0	200	100	60	25	57.978	59.846
42	6	3.0	150	150	110	30	56.854	57.781
43	6	3.0	150	150	75	30	60.050	59.353
44	4	2.0	100	100	90	35	61.948	62.934
45	4	2.0	200	100	90	25	40.329	36.814
46	4	2.0	200	200	60	25	61.948	64.557
47	4	4.0	100	200	60	25	72.884	73.171
48	4	4.0	200	200	90	25	68.689	69.961
49	4	4.0	100	100	90	25	74.232	76.985



Table 3 (continued)

Run	pH	Ads. dose (g/L)	Ini.dye conc. (mg/L)	Rpm	Contact time (min.)	Temp. (°C)	Dye removal (%) exp.	Dye removal (%) pre.
50	4	2.0	100	200	90	25	59.101	62.407
51	8	4.0	200	100	60	35	56.255	53.791
52	1	3.0	150	150	75	30	84.123	79.779
53	6	3.0	150	150	75	30	58.252	59.353

Table 4 ANOVA for fit of dye removal (%) from central composite design

Sources of variation	Sum of squares	Df	Mean square	F-value	P
Regression	5110.83	27	189.29	20.58	0.000
Linear	2848.69	6	474.78	51.62	0.000
Square	521.87	6	86.98	9.46	0.000
Interaction	1740.27	15	116.02	12.61	0.000
Residuals	229.94	25	9.20		
Total	5340.77				

$R^2 = 95.69\%$; R^2 (adjusted) = 91.04%

reliability of the model. 3D surface plots were obtained from the validated model. The obtained F value ($12.72 > F_{\text{critical}}$ 1.94) is 95% significant endorses the model is suitable [31]. R^2 (0.9569) which is near to 1 designates the fit of regression line with the data. From Table 5, the coefficients μ_1 , μ_2 , μ_3 are significant single effects, μ_{11} , μ_{55} , μ_{66} are the significant square effects and μ_{13} , μ_{15} , μ_{16} , μ_{25} , μ_{34} , μ_{36} , μ_{46} are the significant interactive effects as $p < 0.05$.

Interpretation of 3D surface plots

Effect of pH

Adsorbent dose As pH increases dye adsorption decreases this is because at higher pH level, OH^- ions compete with dye anions for active adsorption sites (Fig. 4a). Removal efficiency rises with increase in adsorbent dose due to unsaturated adsorption sites availability. The maximum dye removal is at low pH and increasing adsorbent dose which arguably would increase the positive terminal site at low pH to favor adsorption.

Initial dye concentration Maximum percentage dye removal is obtained at low pH and low dye concentration (Fig. 4b) as dye ions are less than a number of adsorption sites, indicating overlapping of sites (based on PZC value).

RPM Percentage removal of CR dye decreases as pH increases with given RPM (Fig. 4c). This is based on the competition of OH^- ions with negatively charged dye ions. RPM alone does not have much effect on dye removal.

Table 5 Estimated regression coefficients for removal of dye (%)

Term	Coefficient	SE	T	P
μ_0	59.3528	1.0093	58.808	0.000
μ_1	-3.8176	0.4608	-8.284	0.000
μ_2	5.9990	0.4608	13.018	0.000
μ_3	-3.1209	0.4608	-6.773	0.000
μ_4	0.7326	0.4608	1.590	0.124
μ_5	2.1713	0.4608	4.712	0.000
μ_6	-0.4646	0.4608	-1.008	0.323
μ_{11}	2.0057	0.3936	5.096	0.000
μ_{22}	-0.4492	0.3936	-1.141	0.265
μ_{33}	0.7676	0.3936	1.950	0.062
μ_{44}	-0.6081	0.3936	-1.545	0.135
μ_{55}	-1.1907	0.3936	-3.025	0.006
μ_{66}	1.3164	0.3936	3.345	0.003
μ_{12}	-0.0364	0.5361	-0.068	0.946
μ_{13}	1.9034	0.5361	3.550	0.002
μ_{14}	-0.2190	0.5361	-0.409	0.686
μ_{15}	4.3763	0.5361	8.163	0.000
μ_{16}	-1.1797	0.5361	-2.201	0.037
μ_{23}	1.0092	0.5361	1.882	0.071
μ_{24}	-0.5795	0.5361	-1.081	0.290
μ_{25}	3.4821	0.5361	6.495	0.000
μ_{26}	0.3418	0.5361	0.638	0.530
μ_{34}	2.7554	0.5361	5.140	0.000
μ_{35}	-1.0721	0.5361	-2.000	0.057
μ_{36}	1.4783	0.5361	2.757	0.011
μ_{45}	0.4062	0.5361	0.758	0.456
μ_{46}	-2.2752	0.5361	-4.244	0.000
μ_{56}	0.5504	0.5361	1.027	0.314

Maximum removal efficiency is obtained at low pH and high RPM.

Contact time As pH increases dye removal decreases (Fig. 4d) by electrostatic repulsion of dye ions and negatively charged adsorbent according to PZC value of the adsorbent. At high pH as contact time increases removal efficiency of dye molecules increases as sufficient time is available to reach equilibrium.

Temperature At high temperature because of swelling of adsorbent, large dye molecules will penetrate into the adsorbent which intend increases the dye adsorption (Fig. 4e).



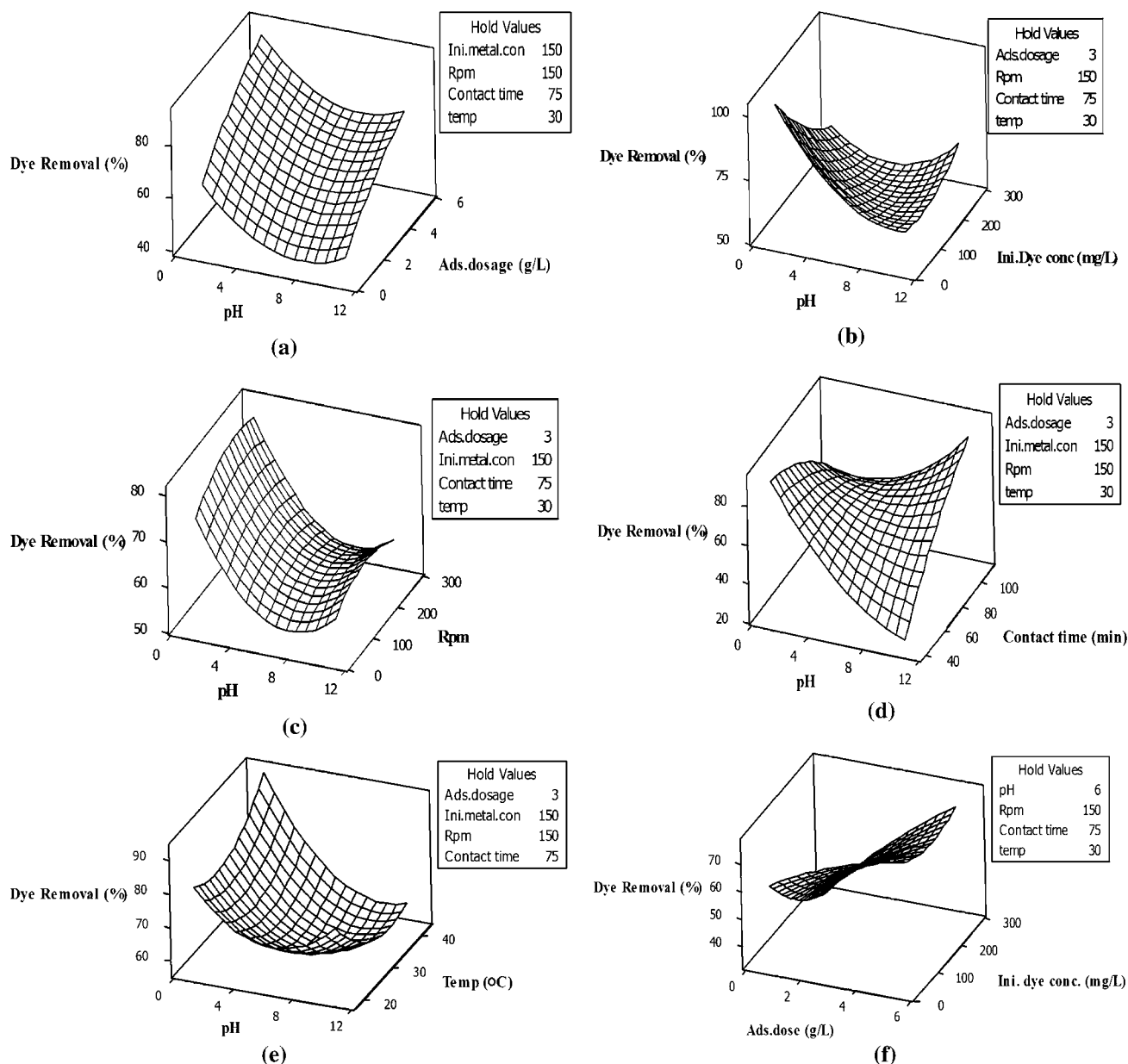


Fig. 4 Interactive effect of **a** pH and adsorbent dose, **b** pH and initial dye concentration, **c** pH and RPM, **d** pH and contact time, **e** pH and temperature and **f** adsorbent dose and initial dye concentration, on removal of CR dye

Same observation is reported in the literature [32]. Maximum dye removal is seen at low pH and high temperature. At high pH region with low-temperature condition removal efficiency increases as mobility of dye molecules decreases which facilitates the adsorption.

Effect of adsorbent dose

Initial dye concentration The vital factor which limits the sorbent–sorbate equilibrium in the system is adsorbent [33].

Figure 4f depicts an increase in the removal of dyes with an increase in adsorbent dose and is maximum at a high dosage. This is attributed as the convenience of sufficient amount of unsaturated adsorbent spots for dye molecules.

RPM From Fig. 5a, it can be noted that RPM alone does not have much effect on percentage dye removal. Maximum adsorption of dye molecules is obtained at high adsorbent dose with given RPM. Since adsorbent dose increases the availability of active adsorption sites also increases which intend increases the adsorption.

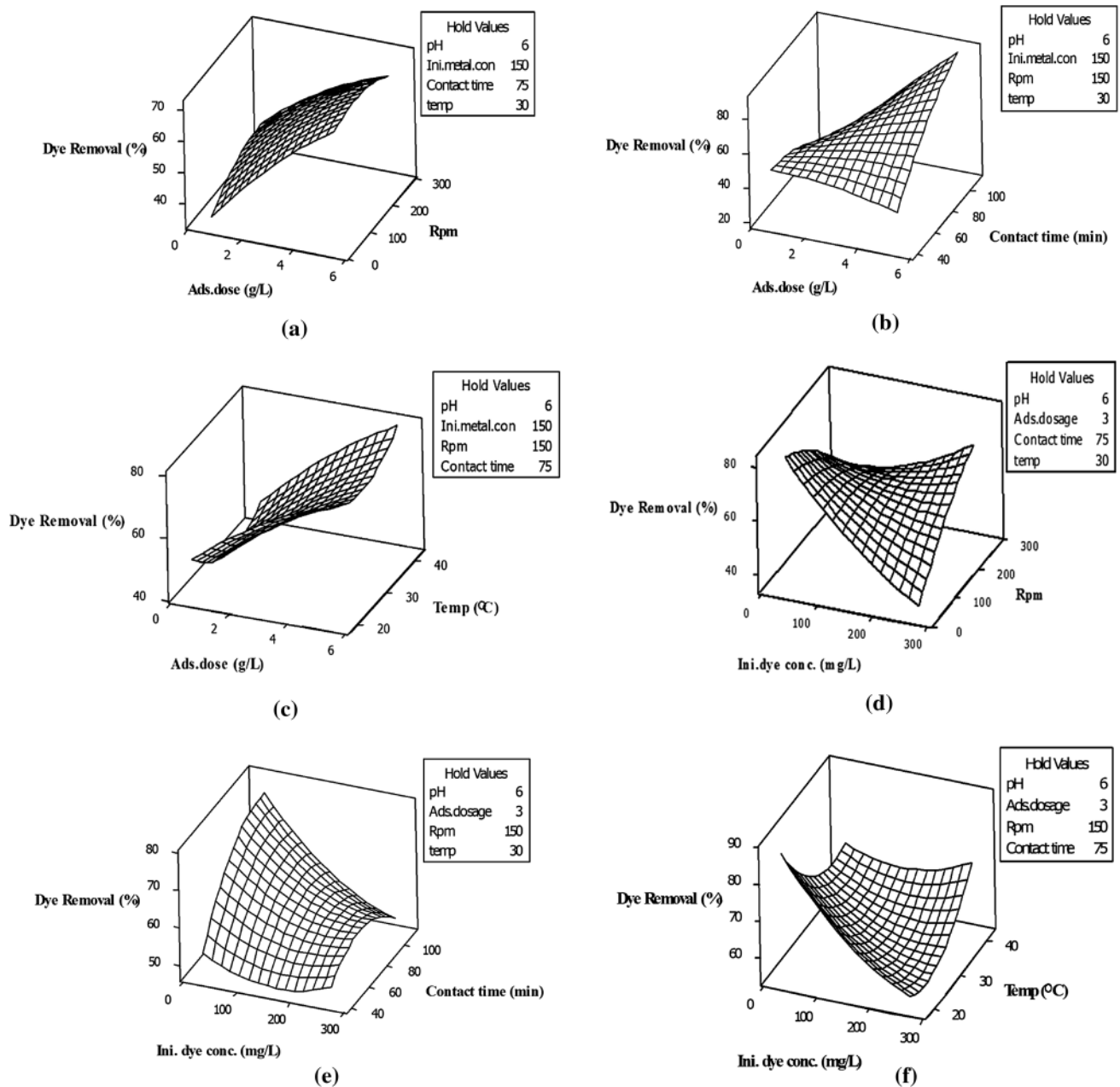


Fig. 5 Interactive effect of **a** adsorbent dose and RPM, **b** adsorbent dose and contact time, **c** adsorbent dose and temperature, **d** RPM and initial dye concentration, **e** initial dye concentration and contact time and **f** initial dye concentration and temperature, on removal of CR dye

Contact time Figure 5b shows at a low dose when contact time increases removal efficiency decreases due to the occurrence of desorption. At high dose, with an increase in contact time adsorption also increases and is maximum at a high dose and high contact time. This is because at high dose, a maximum number of unsaturated adsorption sites are available and sufficient time is available to reach equilibrium.

Temperature Figure 5c shows that as adsorbent dose increases dye adsorption also increases due to an upsurge

in adsorption sites. Dye removal decreases first as temperature increases then increase again. This is because at high-temperature viscosity in the medium decreases which increases the diffusion frequency of the dye molecules into adsorbent pores [34]. Moreover, at low temperature, the mobility of the dye molecules decreases which increases the adsorption process.



Interactions

RPM and initial dye concentration Removal efficiency declines with an increase in the concentration of dye at lesser RPM (Fig. 5d). This is because of non-availability of enough adsorption sites to attain equilibrium. At high RPM with an increase in dye concentration, percentage dye removal also increases. This is attributed to increased concentration gradient (driving force to overcome mass transfer).

Initial dye concentration and contact time Maximum dye removal efficiency is obtained at low concentration and high

contact time (Fig. 5e). This is due to the availability of huge amount of surface capacity for adsorption of dye and enough time for interaction of adsorbent and adsorbate. Removal efficiency decreased at higher adsorbate concentration.

Initial dye concentration and temperature Interactive effect of initial concentration of adsorbate (dye) and the temperature is shown in Fig. 5f. At low temperature, increasing dye concentration decreases the removal rate due to deficiency of adsorption surfaces. As temperature increases surface area of adsorbent increases due to swelling effect which intends increases the adsorption of dye molecules.

RPM and contact time Percentage dye removal increased first with an increase in RPM and then decreases (Fig. 6a). This is because, as RPM increase desorption takes place first and then once again dye molecules adsorbs on the adsorbent. As time increases removal efficiency also increases irrespective of RPM.

RPM and temperature From Fig. 6b it can be noted that the maximum removal is seen at less RPM and high temperature due to increase in pore size of the adsorbent. At high temperature, removal efficiency decreases w.r.t RPM. However, at a lesser temperature, percentage removal increases as RPM increases.

Temperature and contact time At higher temperature, when time improves adsorption of dye molecules also increases and is maximum at high time and temperature. This is because of increase in pore size of adsorbent due swelling effect and availability of sufficient time to reach equilibrium. At low temperature, increasing or decreasing of contact time from mid value has obvious decrease in adsorption of dye molecules (Fig. 6c).

Table 6 presents the comparison of CR dye removal in the present study with the different adsorbents. It can be observed from Table 6 that, the CR dye removal from

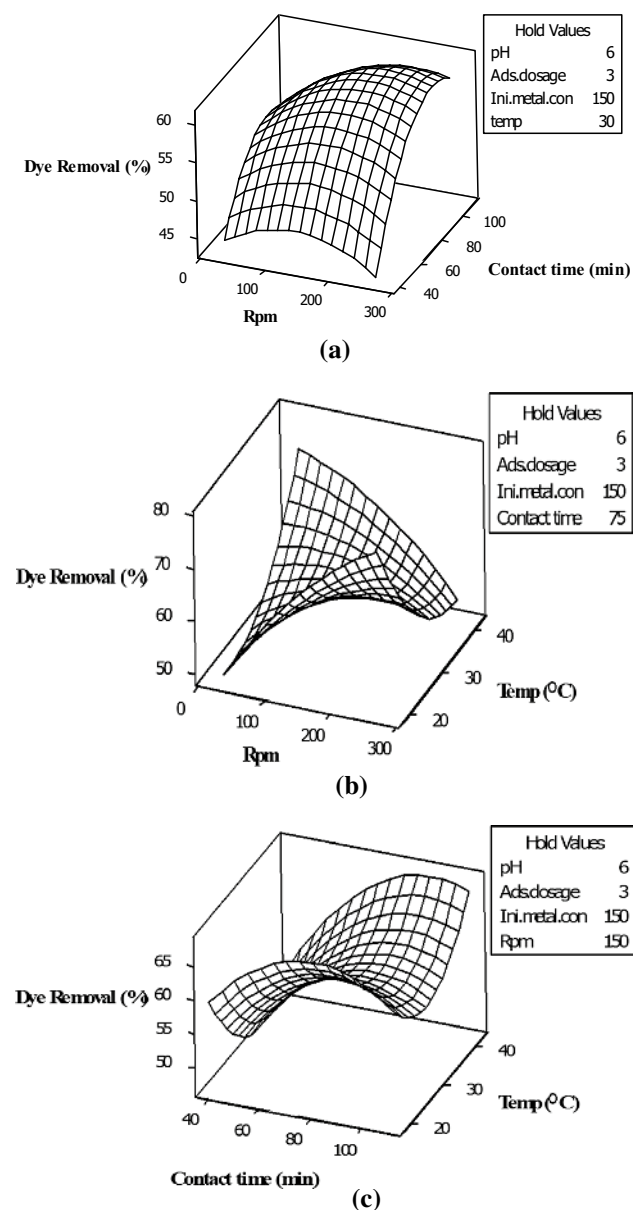


Fig. 6 Interactive effect of **a** RPM and contact time, **b** RPM and temperature, and **c** temperature and contact time, on removal of CR dye

Table 6 Comparison of CR dye removal from aqueous solution by various adsorbents

Adsorbents	Maximum dye removal (%)	References
Australian kaolin	85	[8]
NiO/graphene nanosheets	99.5	[9]
Bottom ash	96.9	[12]
De-oiled soya	97.1	[12]
<i>Eichhornia crassipes</i>	96	[34]
<i>Phragmites australis</i>	98	[35]
Brewers' spent grain	90	[36]
Sawdust activated carbon	96.7	[37]
Natural clay	94	[38]
Burnt clay	98	[39]
Biogas waste slurry	95	[40]
<i>Chrysanthemum indicum</i>	84.1	Present study

aqueous solution by *Chrysanthemum indicum* microparticles is noteworthy and equivalent with other adsorbents reported in the literature.

Conclusion

Chrysanthemum indicum microparticles showed good ability as an adsorbent to reduce the pollutant CR. This study aims to optimize the process parameters of Congo red dye adsorption from chrysanthemum indicum using a CCD which is a RSM module. The optimum condition for maximum dye removal (84.1%) was obtained at pH1, adsorbent dose 0.3 g/100 ml, dye concentration 150 ppm, RPM 150, contact time 75 min and temperature 30 °C. FTIR analysis indicated the formation of new peaks, suggesting the complexation of dye on the surface of the adsorbent. Higher dosage of adsorbent exhibited better removal of CR from the aqueous solution, suggesting that synthesized microparticles can be used as an efficient adsorbent.

Open Access This article is distributed under the terms of the Creative Commons Attribution 4.0 International License (<http://creativecommons.org/licenses/by/4.0/>), which permits unrestricted use, distribution, and reproduction in any medium, provided you give appropriate credit to the original author(s) and the source, provide a link to the Creative Commons license, and indicate if changes were made.

References

- Kaur S, Rani S, Kumar V, Mahajan RK, Asif M, Tyagi I, Gupta VK (2015) Synthesis, characterization and adsorptive application of ferrocene based mesoporous material for hazardous dye Congo red. *J Ind Eng Chem* 26:234–242
- Liu S, Ding Y, Li P, Diao K, Tan X, Lei F, Zhan Y, Li Q, Huang B, Huang Z (2014) Adsorption of the anionic dye Congo red from aqueous solution onto natural zeolites modified with *N,N*-dimethyl dehydrobiethylamine oxide. *Chem Eng J* 248:135–144
- Somasekhareddy MC, Sivaramakrishna L, Varadareddy A (2012) The use of an agricultural waste material, Jujuba seeds for the removal of anionic dye (Congo red) from aqueous medium. *J Hazard Mater* 203–204:118–127
- Bayramoglu G, Akbulut A, Liman G, Arica MY (2017) Removal of metal complexed azo dyes from aqueous solution using tris(2-aminoethyl)amine ligand modified magnetic p(GMA-EGDMA) cationic resin: adsorption, isotherm and kinetic studies. *Chem Eng Res Des* 124:85–97
- Arica TA, Ayas E, Arica MY (2017) Magnetic MCM-41 silica particles grafted with poly(glycidylmethacrylate) brush: modification and application for removal of direct dyes. *Microporous Mesoporous Mater* 243:164–175
- Bayramoglu G, Altintas B, Arica MY (2012) Synthesis and characterization of magnetic beads containing aminated fibrous surfaces for removal of Reactive Green 19 dye: kinetics and thermodynamic parameters. *J Chem Technol Biotechnol* 87:705–713
- Cheng Z, Zhang L, Guo X, Jiang X, Li T (2015) Adsorption behavior of direct red 80 and congo red onto activated carbon/surfactant: process optimization, kinetics and equilibrium. *Spectrochim Acta Part A Mol Biomol Spectrosc* 137:1126–1143
- Vimonses V, Lei S, Jin B, Chow CWK, Saint C (2009) Adsorption of congo red by three Australian kaolins. *Appl Clay Sci* 43:465–472
- Rong X, Qiu F, Qin J, Zhao H, Yan J, Yang D (2015) A facile hydrothermal synthesis, adsorption kinetics and isotherms to Congo Red azo-dye from aqueous solution of NiO/graphene nanosheets adsorbent. *J Ind Eng Chem* 26:354–363
- Chatterjee S, Chatterjee S, Chatterjee BP, Guha AK (2007) Adsorptive removal of congo red, a carcinogenic textile dye by chitosan hydrobeads: binding mechanism, equilibrium and kinetics. *Colloids Surf A Physicochem Eng Asp* 299:146–152
- Zvezdelina Yaneva VN (2012) Insights into Congo red adsorption on agro-industrial materials—spectral, equilibrium, kinetic, thermodynamic, dynamic and desorption studies. A review. *Int Rev Chem Eng* 4:127
- Mittal A, Mittal J, Malviya A, Gupta VK (2009) Adsorptive removal of hazardous anionic dye “Congo red” from wastewater using waste materials and recovery by desorption. *J Colloid Interface Sci* 340:16–26
- Shu J, Wang Z, Huang Y, Huang N, Ren C, Zhang W (2015) Adsorption removal of Congo red from aqueous solution by polyhedral Cu₂O nanoparticles: kinetics, isotherms, thermodynamics and mechanism analysis. *J Alloys Compd* 633:338–346
- Bhaumik M, McCrindle R, Maity A (2013) Efficient removal of Congo red from aqueous solutions by adsorption onto interconnected polypyrrole-polyaniline nanofibres. *Chem Eng J* 228:506–515
- Zhang Z, Moghaddam L, O’Hara IM, Doherty WOS (2011) Congo Red adsorption by ball-milled sugarcane bagasse. *Chem Eng J* 178:122–128
- Pavan FA, Dias SLP, Lima EC, Benvenutti EV (2008) Removal of Congo red from aqueous solution by anilinepropylsilica xerogel. *Dye Pigment* 76:64–69
- Somasekhareddy MC (2006) Removal of direct dye from aqueous solutions with an adsorbent made from tamarind fruit shell, an agricultural solid waste. *J Sci Ind Res (India)* 65:443–446
- Deng L, Zeng H, Shi Z, Zhang W, Luo J (2018) Sodium dodecyl sulfate intercalated and acrylamide anchored layered double hydroxides: a multifunctional adsorbent for highly efficient removal of Congo red. *J Colloid Interface Sci* 521:172–182
- Yu Z, Liu B, Zhou H, Feng C, Wang X, Yuan K, Gan X, Zhu L, Zhang G, Xu D (2017) Mesoporous ZrO₂ fibers with enhanced surface area and the application as recyclable absorbent. *Appl Surf Sci* 399:288–297
- Zheng Y, Wang H, Cheng B, You W, Yu J (2018) Fabrication of hierarchical bristle-grass-like NH₄Al(OH)₂CO₃@Ni(OH)₂ core-shell structure and its enhanced Congo red adsorption performance. *J Alloys Compd* 750:644–654
- Lei C, Pi M, Xu D, Jiang C, Cheng B (2017) Fabrication of hierarchical porous ZnO-Al₂O₃ microspheres with enhanced adsorption performance. *Appl Surf Sci* 426:360–368
- Chen H, Zheng Y, Cheng B, Yu J, Jiang C (2018) Chestnut husk-like cobaltite hollow microspheres for the adsorption of Congo red. *J Alloys Compd* 735:1041–1051
- Bayramoglu G, Arica MY (2018) Adsorption of Congo Red dye by native amine and carboxyl modified biomass of *Funalia trogii*: isotherms, kinetics and thermodynamics mechanisms. *Korean J Chem Eng* 35(6):1303–1311
- Liu PL, Wan Q, Guo YP, Yang J, Rao GY (2012) Phylogeny of the genus *Chrysanthemum* L.: evidence from single-copy nuclear gene and chloroplast DNA sequences. *PLoS One*. <https://doi.org/10.1371/journal.pone.0048970>



25. Vilvanathan S, Shanthakumar S (2016) Ni (II) adsorption onto *Chrysanthemum indicum*: influencing factors, isotherms, kinetics, and thermodynamics. *Int J Phytoremediation* 18:1046–1059
26. Chukki J, Shanthakumar S (2016) Optimization of malachite green dye removal by *Chrysanthemum indicum* using response surface methodology. *Environ Prog Sustain Energy* 35:1415–1419
27. Saeed MO, Azizli K, Isa MH, Bashir MJK (2015) Application of CCD in RSM to obtain optimize treatment of POME using Fenton oxidation process. *J Water Process Eng* 8:e7–e16
28. Chaudhary N, Balomajumder C (2014) Optimization study of adsorption parameters for removal of phenol on aluminum impregnated fly ash using response surface methodology. *J Taiwan Inst Chem Eng* 45:852–859
29. Ghorai S, Sarkar AK, Panda AB, Pal S (2013) Effective removal of Congo red dye from aqueous solution using modified xanthan gum/silica hybrid nanocomposite as adsorbent. *Bioresour Technol* 144:485–491
30. Roy P, Mondal NK, Das K (2014) Modeling of the adsorptive removal of arsenic: a statistical approach. *J Environ Chem Eng* 2:585–597
31. Hassani A, Soltani RDC, Karaca S, Khataee A (2015) Preparation of montmorillonite–alginate nanobiocomposite for adsorption of a textile dye in aqueous phase: isotherm, kinetic and experimental design approaches. *J Ind Eng Chem* 21:1197–1207
32. Khodam F, Rezvani Z, Amani-Ghadim AR (2015) Enhanced adsorption of Acid Red 14 by co-assembled LDH/MWCNTs nanohybrid: optimization, kinetic and isotherm. *J Ind Eng Chem* 21:1286–1294
33. Gohari M, Hosseini SN, Sharifnia S, Khatami M (2013) Enhancement of metal ion adsorption capacity of *Saccharomyces cerevisiae*'s cells by using disruption method. *J Taiwan Inst Chem Eng* 44:637–645
34. Wanyonyi WC, Onyari JM, Shiundu PM (2014) Adsorption of Congo Red dye from aqueous solutions using roots of *Eichhornia crassipes*: kinetic and equilibrium studies. *Energy Procedia* 50:862–869
35. Omran AR, Baiee MA, Juda SA, Salman JM, Alkaim AF (2016) Removal of Congo red dye from aqueous solution using a new adsorbent surface developed from aquatic plant (*Phragmites australis*). *Int J ChemTech Res* 9:334–342
36. Kezerle A, Velic N, Hasenay D, Kovacevic D (2018) Lignocellulosic materials as dye adsorbents: adsorption of Methylene Blue and Congo Red on Brewers' spent grain. *Croat Chem Acta* 91:53–64
37. Kini MS, Prabhu KB, Gundecha A, Devika U (2017) Statistical analysis of Congo Red dye removal using sawdust activated carbon. *Int J Appl Eng Res* 12:8788–8804
38. Bentahar S, Dbik A, El-khomri M, El-messaoudi N, Bakiz B, Lacherai A (2016) Study of removal of Congo red by local natural clay. *St Cerc St CICBIA* 17:295–307
39. Mumin MA, Khan MMR, Akhter KF, Uddin MJ (2007) Potentiality of open burnt clay as an adsorbent for the removal of Congo red from aqueous solution. *Int J Environ Sci Technol* 4:525–532
40. Namasivayam C, Yamuna RT (1992) Removal of Congo red from aqueous solutions by biogas waste slurry. *J Chem Tech Biotechnol* 53:153–157

Publisher's Note Springer Nature remains neutral with regard to jurisdictional claims in published maps and institutional affiliations.

